Focal Ratio Degradation in Optical Fibres

Vincent van Assen
Supervisor: prof.dr. M.A.W. Verheijen

November 25, 2011

Abstract

The properties of optical fibres used in spectroscopic instruments are influencing the instrument design. In this bachelor research project we developed a simple experimental set-up to measure the focal ratio degradation and its dependence on the curvature of the fibre and the length of the fibre. We found that losses in both resolution and in efficiency are unavoidable with the use of the studied fibres. This research also shows that macrobends are not influencing the focal ratio degradation characteristics of the fibre in such a way that this has to be taken into account in the optical design of the instrument.

Contents

1 Introduction

Integral Field Spectrography (IFS) is a technique widely used in astronomy which provides spectra for a large number of spatial elements within a two-dimensional field of view, rather than a conventional one-dimensional spectrograph. Fibre optics made it possible to remove the relative heavy spectrographs from the back of telescopes. In these fibre based instruments a bundle of fibres is placed in the focal plane of the telescope. These fibres which lead to the spectrograph are then put into a row which forms the spectrograph slit. By using this type of instrument simultaneously a large number, dependent on the number of fibres, of spectra can be measured. This makes it possible to obtain high resolution spectrographic radial velocity determinations and not least a series of spectra in just one exposure time, which makes the measurements considerably cheaper.This allows for example to determine the Disk Mass of low surface brightness spiral galaxies by measuring the velocity dispersion with high precision (Verheijen et al. 2004)[2].

This project report describes how we characterized the fibres to be used in the Integral Field Spectrograph or Integral Field Unit (IFU) for the 'Gratama Telescope' located at the 'De Blaauw observatory' in Groningen the Netherlands. This observatory is located at one of the university buildings in Groningen and consists of two stories. The 40 cm telescope is located on the top floor, and the control room and the spectrograph room are located on the floor below. In order to be able to perform integral field spectrography, a 13 metre long optical fibre bundle has to be made from the telescope to the spectrograph room one story below. The IFU contains a bundle of 75 fibres, containing science-fibres, calibration-fibres and spare-fibres.

The use of optical fibres brings additional difficulties in the optical system design of the IFU. Obviously the light propagated by the optical fibre comes out differently than it entered the fibre. The largest and most unwanted effect of the fibre is called Focal Ratio Degradation (FRD). Generally FRD means that the incoming cone of light is smaller than the outcoming cone of light. FRD is caused by diffraction and surface irregularities on the fibre wall, these factors all tend to decollimate the incoming light making it necessary to increase collimator sizes at the spectrograph to keep the efficiency of the system high. Increasing the collimator size is not just costly, but is also decreasing the resolution of the instrument. In this research we measured the FRD of the optical fibre used at the Blaauw Observatory in Groningen, to be able to construct an adequate optical system for the integral field spectrograph. Because the fibre will have to be able to follow the telescope's movements by tracking the object of interest, the bends in the fibre will vary for different positions of the telescope. Therefore we did measurements on the fibre while it was bent with different radii of curvature.

This research contains four parts, the first part describes the theory of fibre optics and FRD. In the second part the fibre, experimental set-up, fibre preparations and the measurements are presented and in the third part the results of the measurements. Finally in the fourth part we discuss the results, their implications for the instrument design combined with the conclusions that can be drawn from the research.

2 Theory

2.1 Fibres

Fibres are optical wave guides used for a variety of purposes, and a wide range of different fibres are manufactured mostly for communication purposes. In 1955 the first suggestions were made by Kapany to use optical fibres for astronomical use. He suggested to use an assembly of fibres to transform the shape of a beam of light by assembling a bundle of fibres at the star image and assemble the other fibre ends in a row to form the slit of the spectrograph [4].

As mentioned, fibres are manufactured for different purposes and with different characteristics. Fibres are generally made from silica with a transparant, low index cladding surrounding the core. Characteristics of the fibre depend upon the core diameter and the used material. Generally fibres with a large core are multimode fibres used for short distance (<1 km) communication. Single-mode fibres contain a much smaller core and are used for long distance (>1 km) light propagation. Figure 1 shows the different lay out of a multi-mode and a single-mode fibre.

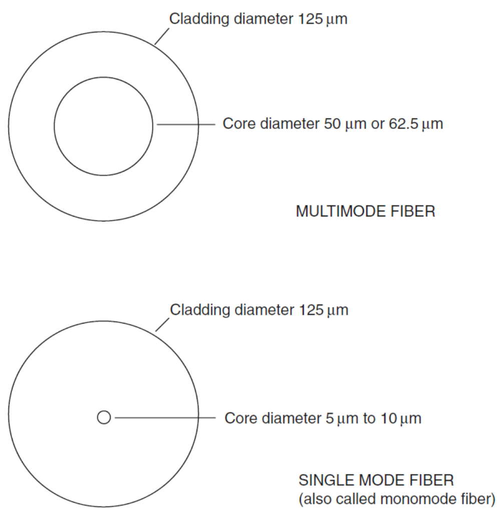

Figure 1: Multi-mode and mono-mode fibres [1]

For astronomical purposes, fibre lengths are generally below 100 metres. From that perspective a multi-mode fibre is applicable. Apart from the fact that the guiding distance of the light is short, we are generally interested in propagating the light from an image of the telescope to the spectrograph. Single-mode fibres are therefore less applicable since they will only propagate the light that falls perpendicularly to the fibre ends surface. This research is limited to multi-mode, step index fibres.

Unless the fibre is an optically ideal fibre, the light propagated by the fibre is affected by the travel through the waveguide. The most important effects are mode scrambling and FRD. Both effects are losses. Especially FRD affects the entire instrument design for the IFS. FRD 'speeds up' the incident focal ratio and the result is that the optics at the spectrograph side of the fibres has to increase in size to maintain (into some amount) the efficiency of the optical system. A major drawback from increasing the optics is the decrease of the throughput-resolution. Since the spectrograph slit is limited in size this means that less fibres can be attached to the spectrograph in the same time. To increase the number of fibres, a larger spectrograph is needed which is more expensive. This means FRD is a loss in both optical terms and financial terms. The need to minimize the FRD for the fibres is therefore necessary to design an efficient and cost effective instrument.

2.2 Modes

A fibre contains modes which depend on the core diameter and the refractive index of the fibre core and cladding. These modes are plain waves incident at a certain angle Θ to the fibre axis and can be divided in lossy and propagating modes, see figure 2 for a schematic figure of modes in a multi-mode single index fibre.

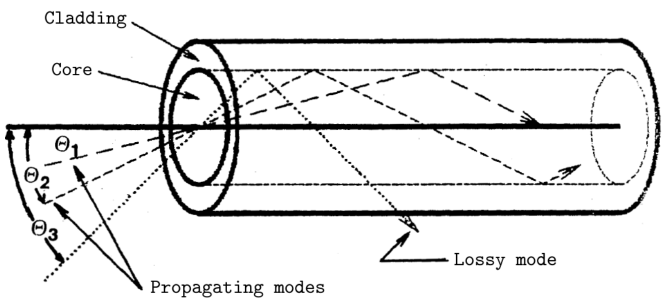

Figure 2: Different modes [6]

2.3 Losses

Losses in optical fibres can be divided into two types: mode independent and mode dependent losses. Mode independent losses are due to material absorption and scattering, both have a spectral dependence. Material impurities at the core are the main drivers of these losses. In the fibre specifications in appendix A, it can be seen that a peak arises at around 1380nm. This peak is dedicated to hydroxyl ions in the core. The other smaller peaks are due to metallic traces in the fibres [1]. Rayleigh scattering also plays a role and becomes more dominant at shorter wavelengths, which is obviously an implication of the $1/\lambda^4$ dependence of Rayleigh scattering. This effect can also be found in the plot in appendix A. Both scattering and absorption by impurities set limits to the spectral windows of the instrument but do not affect the optical design of the instrument.

Mode dependent losses do affect the optical design of the instrument. These losses are caused by two mechanisms: the first is waveguide scattering and mechanical deformation.[6] Waveguide scattering can scatter propagating modes into lossy modes which causes energy loss to the cladding. Apart from this energy loss, light also gets scattered into modes with a bigger angle with respect to the fibre axis, which causes a large exit angle. This is in fact FRD. As mentioned before, the optics of the instrument have to increase in size to keep the efficiency high due to FRD influencing the optical design. Waveguide scattering is mainly caused by variation of the core diameter along the fibre axis, this effect also contributes to FRD.

Mechanical deformation is the offset from the fibre with respect to a straight cylinder, this deformation can occur in two varieties. Large scale bending, or macrobending, applies when the radius of curvature of the fibre is large with respect to the core diameter. Small scale bendings, or microbending, are situations in which the radius of curvature of the deformation is small in comparison with the fibre core diameter.

Figure 3 gives a schematic impression of the FRD caused by macrobending. The fibre in the drawing is fed with one single mode, this mode is azimuthally dispersed. Azimuthal dispersion is not a major issue in the instrument design, it is the radial dispersion, in the picture denoted as $\Delta\Theta$ which is in fact the Focal Ratio Degradation. Since the input mode does not necessarily comes out of the fibre with the same focal ratio. Radial dispersion by macrobends is described in a formula by Ramsey in 1988 [6] by equation 1.

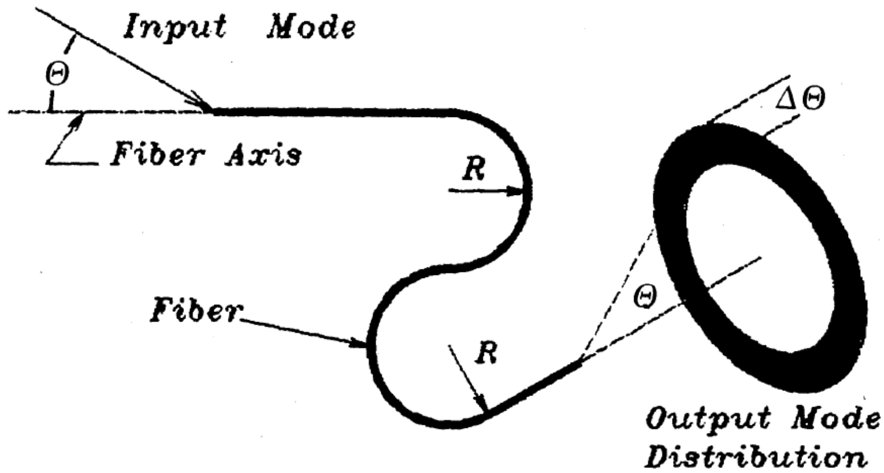

Figure 3: Dispersion of a single mode by macrobending [6]

$$\Delta\Theta/\Theta = d/R \tag{1}$$

In this formula d is the core diameter, R is de radius of curvature as in figure 3, Θ is the angle with respect to the fibre axis of the incident light wave and $\Delta\Theta$ is the radial dispersion. Apart from macrobending, microbending also has a small contribution to FRD, but even more important the transmission of the fibre decreases due to energy losses to the cladding.

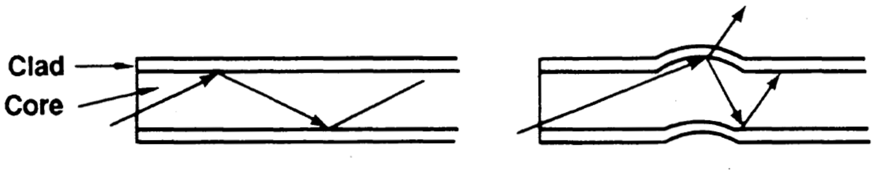

Figure 4: Schematic representation of microbending [7]

As can be seen in figure 4, microbends reflect light into lossy modes, this causes additional losses to the spectral losses which we discussed before. Apart from losing light, a fraction of the light is scattered in an extreme mode. This causes a ray which will exit the fibre with a large angle with respect to the fibre axis. This adds up to the FRD caused by macrobending. In the design of the instrument, microbending has to be avoided as much as possible because the effects of these tiny stresses to the fibre affect the efficiency of the instrument significantly. Macrobending is obviously unavoidable since the telescope's movement causes bending and the fibre has to bridge the distance between the telescope and the spectrograph which can not be done without any bends.

2.4 Numerical Aperture

As can be seen in figure 2, not all modes are resulting in the propagation of light through the fibre. When we assume the fibre as being an ideal optical system we can define a cone of acceptance or numerical aperture (NA), which can be calculated by equation 2. The NA contains all the modes for which incident light to the face of the core will be propagated by the core of the fibre, see figure 5.

$$NA = \sqrt{n_{core}^2 - n_{cladding}^2} \tag{2}$$

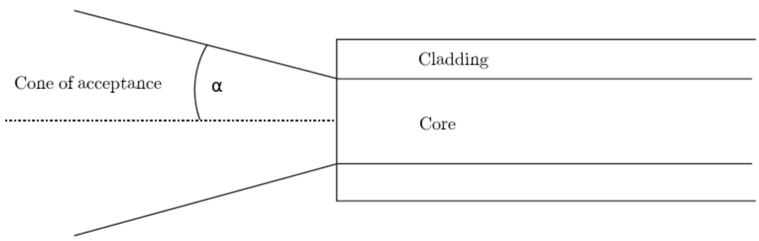

Figure 5: Acceptance cone (or Numerical Aperture) [1]

Like many physical processes, ideal fibres do not exist and the formula is a description of an ideal situation. For real fibres, therefore, the NA is just a rough estimate. In fact the NA is slightly smaller than described by equation 2 since the modes that are just in the cone of acceptance are turned into lossy modes due to scattering, macrobends and microbends.

3 Method

3.1 Used fibre

For this research the Polymicro FBP200220240 was used. This fibre is a Broad Spectrum Optical Fibre. For the characteristics provided by the manufacturer see appendix A. The fibre has a core made from silica with a diameter of 200 μm, a cladding made from doped silica with an outer diameter of 220 μm and a buffer to protect from mechanical impact with an outer diameter of 240 μm. The fibre has a NA of 0.22, this means that the maximum input focal ratio for this particular fibre is around F2.3. As described in section 3.4, we did not perform measurements with the fibre illuminated at this focal ratio.

3.2 Experimental set-up

To measure the FRD in the proposed fibre, the following experiment was developed. Since we are interested in the FRD for different incoming focal ratios, an optical system was designed in which different diafragmas could be inserted to illuminate the fibre end with the preferred focal ratio. It was important that the light source was uniform over the area we used to illuminate the fibre. Therefore a uniform source integrating sphere with a halogen lamp was built. Integrating spheres are efficient in scattering the light uniformly over the wall of the sphere, and as long as the output port is relatively small to the radius of the sphere, the output over this port is uniform.

A pinhole was placed right in front of the output port of the uniform source integrating sphere. Then a collimating lens was used to collimate the light onto the second lens with the same properties. This second lens was used to focus the light on the fibre end. Both lenses were plano convex with their focus at 120 mm. Inbetween the two lenses a replaceable aperture was placed to change the input focal ratio of the fibre.

At the other end the fibre was placed carefully against the protecting glass sheet of the CCD camera. To reduce the effect of background light, the camera, a SBIG ST-7, and the fibre end were shielded with a black cardboard box. The distance between the fibre end, located against the protecting glass sheet, and the CCD imaging plane are known and can be found in the technical details of the CCD, see figure 7. The illuminated fibre end, as well as the diafragma and lenses, were located on an optical rail to ensure all optical elements were aligned properly and the distances between the optical elements could be set accurately. In figure 6 a schematic overview of the fibre illumination set-up is given, in figure 8 a photo of the experimental set-up can be found. In figure 7 a schematic overview of the fibre end at the CCD end is shown and in figure 9 a picture of the CCD end of the fibre. The CCD we have used was built with a thinner front plate than mentioned in the text in the figure. The protective glass sheet lies a little behind the front plate. This distance was measured to be 1.0 mm. This makes the distance between the fibre end and the imaging plane of the CCD 16.5 mm.

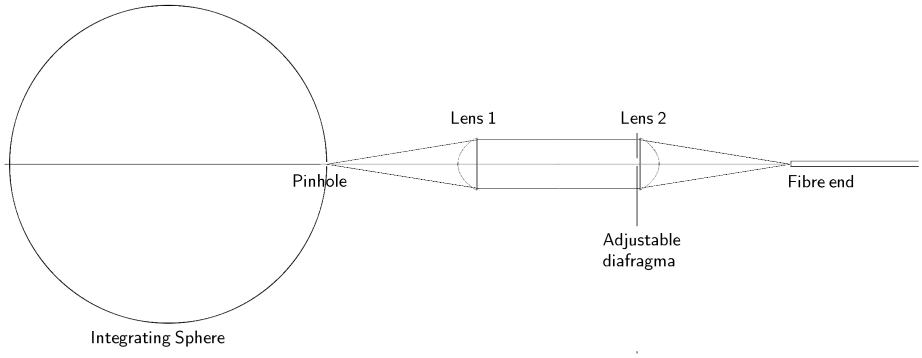

Figure 6: Optical design for fibre illumination

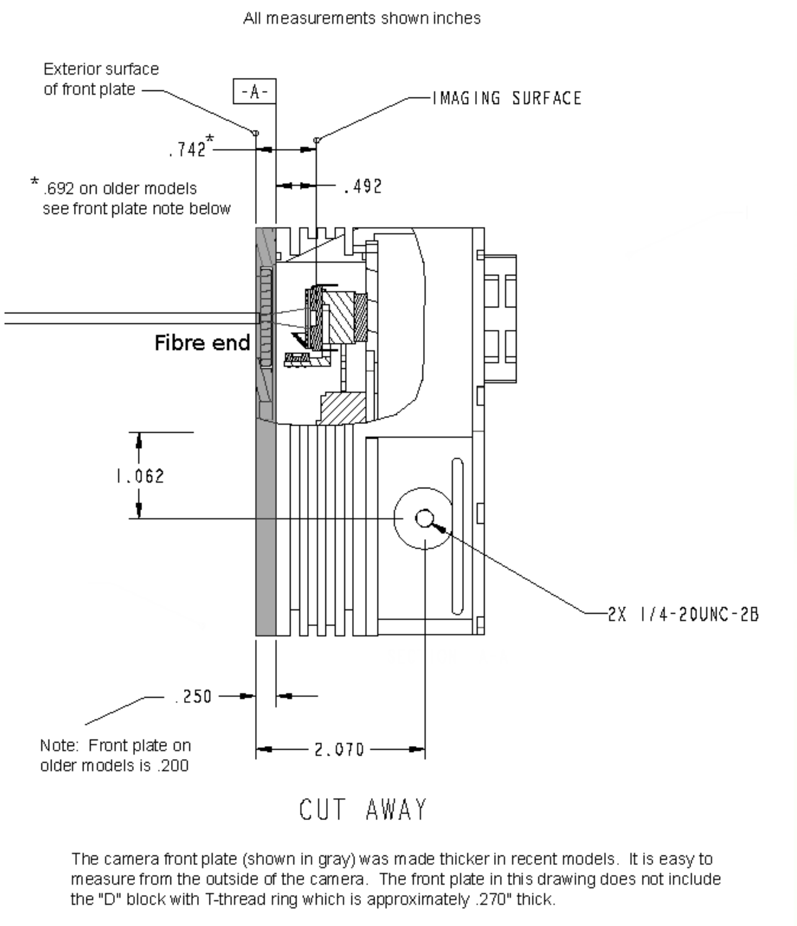

Figure 7: CCD end of the fibre

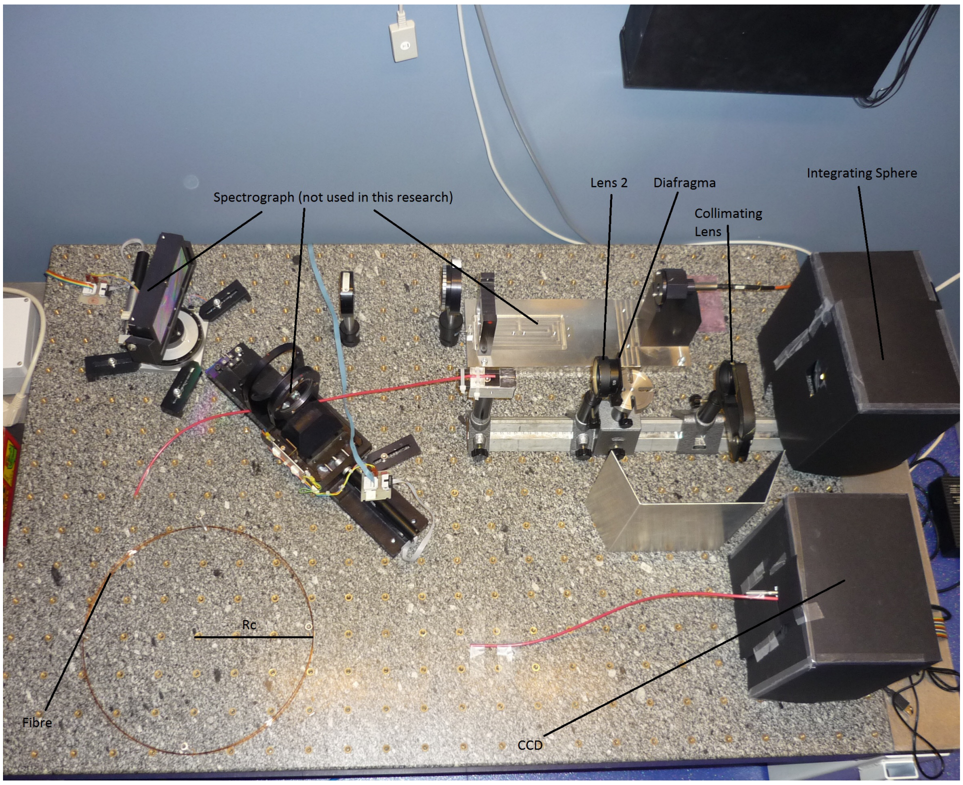

Figure 8: Photo of the experimental set-up

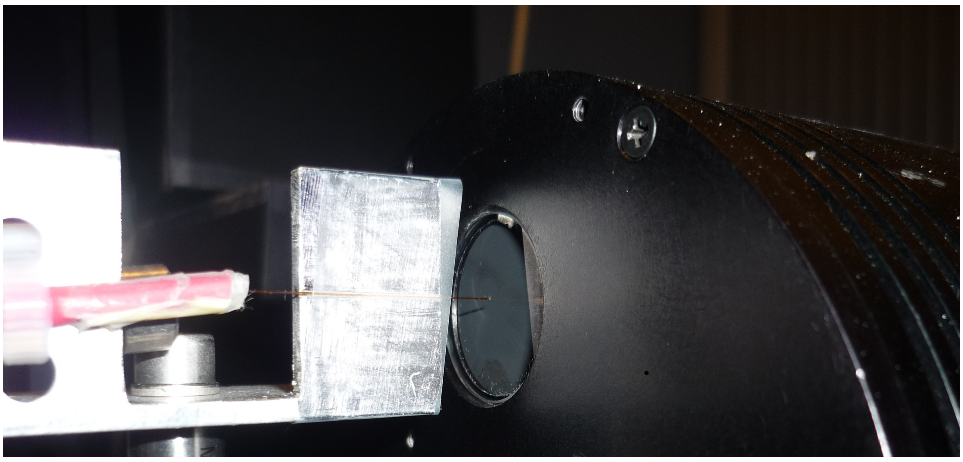

Figure 9: Fibre end placed against the protective glass sheet of the CCD

3.3 Fibre preparation

For the measurements described in the next section, one fibre of 2 metres and one fibre of 13 metre (the needed length for the instrument) were prepared. To make sure no additional scattering effects would occur at rough fibre ends, the fibres had to be polished and checked for faults. The polishing process was performed with a hollow needle, which was placed around the fibre and fixed into a small drilling head and an aluminium cone to hold the fibre mount. In this way the fibre was mounted perpendicularly to the polishing pad.

The polishing procedure was done in 4 steps, during step 1 the fibre was polished on waterproof 3M P1200 sandpaper, during this step the fibre end was polished flat and major faults were scoured away. During steps 2, 3 and 4 the fibre end was polished on respectively 3, 1 and 0.3 μm grain size aluminium oxide polishing pads. In the last steps the fibre end was polished untill no faults were seen anymore using a microscope with a 400 times magnification. For convenience a webcam was attached to the microscope to visualise the fibre ends. The pictures in figure 10 were made with this setup. As can be seen in Figure 10 the fibre ends, at this magnification (400 times), show no contaminations or faults anymore. In the right of the two pictures one can see the cladding and the buffer around the lit core of the fibre. The vague shadows around the buffer of the fibre are contaminations of the polishing process on the buffer away from the fibre end.

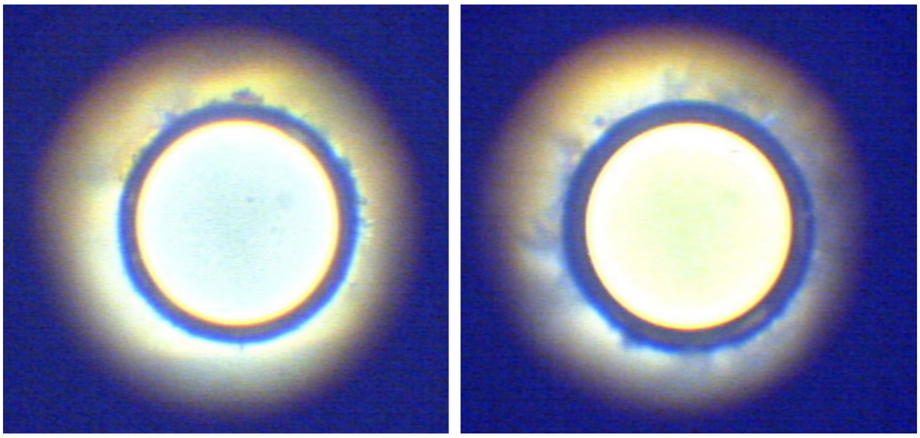

Figure 10: Two fibre ends, left polished with 1 μm pad and right polished with 0.3 μm pad.

3.4 Measurements

In the optical set-up different lengths of fibres can be attached. While attached, the radius of curvature of the fibre can be changed without moving the fibre ends. This makes it possible to perform consistent measurements with a variable radius of curvature. Apart from the radius of curvature, the adjustable diafragma can be changed. To make sure the diafragma sizes remain consistent over the different measurements, fixed diafragmas were made out of aluminium plates. These apertures where chosen in such a way that the focal ratio varied between 3 and 20. Table 1 shows the different aperture sizes and their corresponding focal ratio. Since the telescope beam is F/8, the apertures were chosen in such a way that a number of measurements around F/8 could be performed. Nevertheless, focal ratios different from F/8 are also interesting, since fore optics might be applied to increase the plate scale of the telescope in the future.

Aperture size	Focal ratio	Integration time
6	20	5.000
8	15	2.813
10	12	1.800
12	10	1.250
13	9.23	1.070
14	8.57	0.920
15	8	0.800
16	7.5	0.703
18	6.67	0.556
20	6	0.450
24	5	0.313
30	4	0.20
40	3	0.120

Table 1: Aperture sizes for performed measurements

To make sure no light was lost in the experimental set-up, the integration times for the different diafragmas were normalised. Meaning that the amount of light exposed on the fibre in a 5 second integration time with a 6mm diafragma, equals the amount of light exposed on the fibre end with a bigger diafragma. This results in an integration time as a function of the aperture size as in equation 3 with d the diafragma diameter and a a constant, the integration times used can be found in the third column in table 1. During the data reduction the total output light of the fibre was calculated and compared to the other measurements.

$$\pi d^2 t_{exp} = a \rightarrow t_{exp} = \frac{a}{\pi d^2} \tag{3}$$

3.5 Data reduction

In the described experimental set-up .fit files were made from the different light exposures and fibres. Typically this results in pictures like the one in figure 11. From these pictures the centre of the bright spot was calculated. After that, the picture was loaded into Gipsy and with the Ellint command tables were produced with the mean of the number of counts falling into donut shaped apertures around the centre with a width of 1 pixel. In the same step color maps with the marked centre were made. The marks were used to visually check if the centre was calculated correctly.

Figure 12 shows, for four different input focal ratios, the resulting color maps. As can be seen in the bottom right picture, not all the light exiting the fibre falls on the CCD. Ellint calculates the average of the pixels illuminated and extrapolates the light for the parts of the donuts which are larger than the

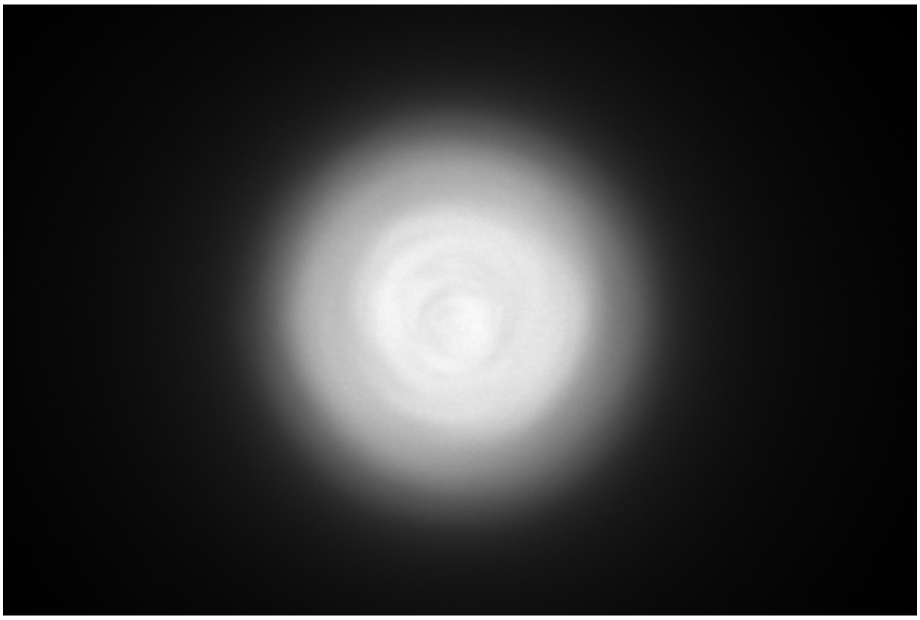

Figure 11: Typical output from the set-up

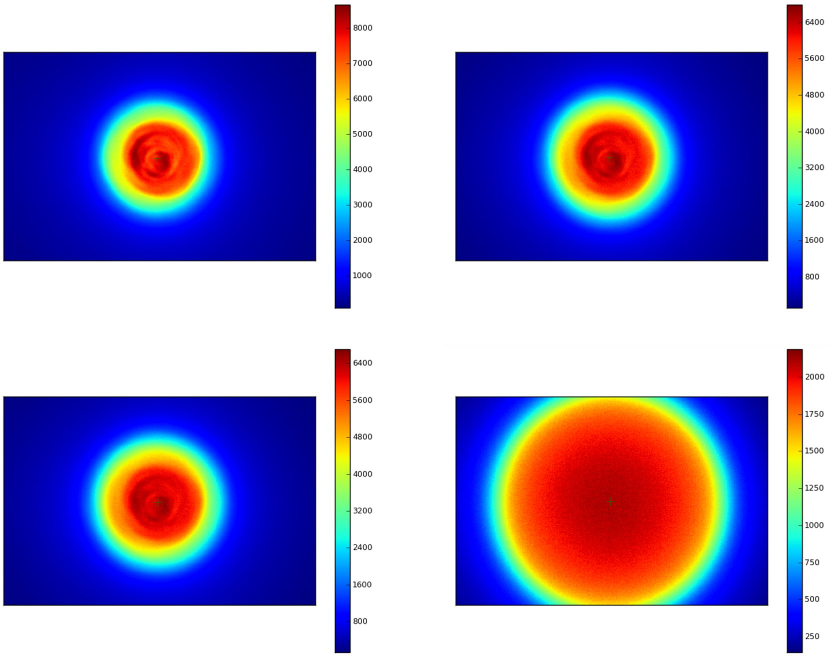

Figure 12: Four different results for fibres, the upper left is a fibre exposed to a F/20 beam, the upper right is exposed to a F/10 beam, bottom left to a F/8 beam and the bottom right to a F/3 beam.

CCD. This method makes the output less reliable and will be taken into account in the discussion later on in this report.

In all the measurements, we make the rough assumption that all the light incident to the fibre end is transmitted by the fibre. This makes all our calculations and conclusions relative in nature, absolute measurements are not an option in the experimental set-up described above. The data files created with the Ellint tool were used to make radial plots of the illumination of the CCD by the fibre end. These files were also used to calculate the total amount of light coming from the fibre end, and could be used to define a radius within which a certain amount of light is emitted. Since the plate scale of the CCD is known, as well as the distance between the fibre end and the imaging plane of the CCD, the focal ratio can be determined.

4 Results

4.1 Light losses

As described earlier, the integration times were adjusted to the diafragma apertures in order to keep the amount of light constant for the different measurements. In figures 13 and 14 radial plots are given for two runs of measurements.

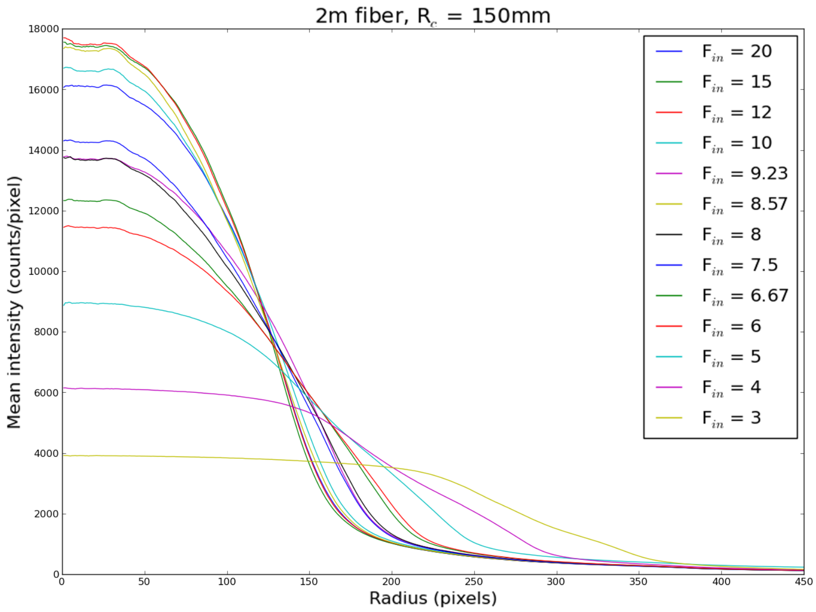

Figure 13: Radial intensity for measurements on a 2 metre fibre with a radius of curvature of 150 mm

Figure 15 shows the radial intensity plots for both the 2 metre fibre and the 13 metre fibre with different radii of curvature, all fed with a F/8 input beam. Note that the $R_c = 100$ mm of the 13 metre fibre is significantly lower in intensity than the other measurements. This might be caused by microbends or due to the fact that the fibre was rolled up several times with a radius of curvature of 100 mm to store the long fibre.

What can be seen is that the total throughput of the fibres differs, the 2 metre fibre has its maximum at 18 000 counts and the 13 metre at 12 000. The integrated intensities of the measurements are tabulated in table 4.1.

Note the ‘wiggles’ in the radial intensity plots in figure 14, these are due to the fact that in this fibre not all modes are filled when illuminated by a high focal ratio beam. As can be seen these modes are all filled when the fibre is illuminated with a low focal ratio beam.

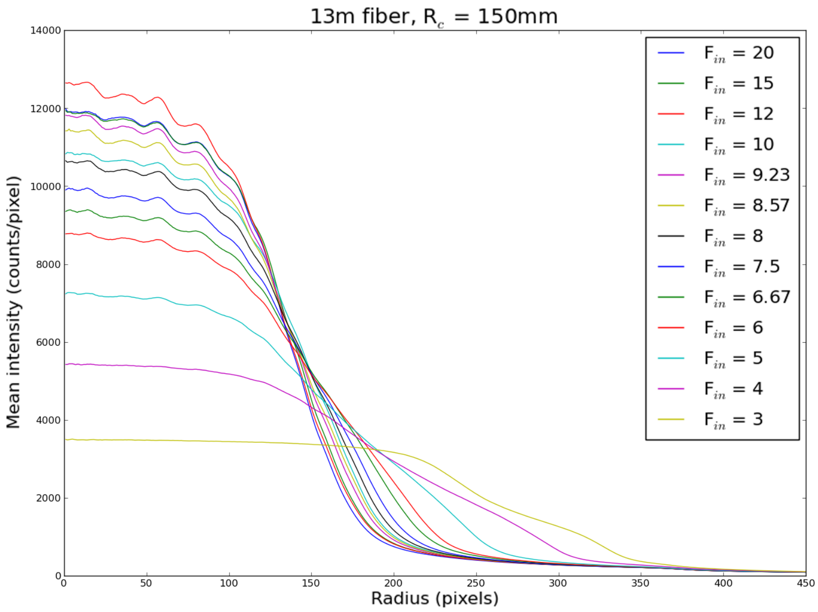

Figure 14: Radial intensity for measurements on a 13 metre fibre with a radius of curvature of 150 mm

F/# in	Exposure time (sec.)	Total light, 2m fibre	Total light, 13m fibre
20	5.000	1.02987473e+09	8.67500339e+08
15	2.813	1.05048710e+09	8.92398629e+08
12	1.800	1.06128865e+09	8.97516327e+08
10	1.250	1.07076496e+09	8.99648671e+08
9.23	1.070	1.06234045e+09	8.98114680e+08
8.57	0.920	1.05607147e+09	8.95177940e+08
8	0.800	1.04363915e+09	8.94337201e+08
7.5	0.703	1.04228220e+09	8.88141206e+08
6.67	0.556	1.06752804e+09	9.07121875e+08
6	0.450	1.06503890e+09	9.08284208e+08
5	0.313	1.12074650e+09	9.01469466e+08
4	0.200	1.06032514e+09	9.06688398e+08
3	0.120	1.05469200e+09	8.83121237e+08

Table 2: Integrated intensities for 2 and 13 metre fibres with different input F/#

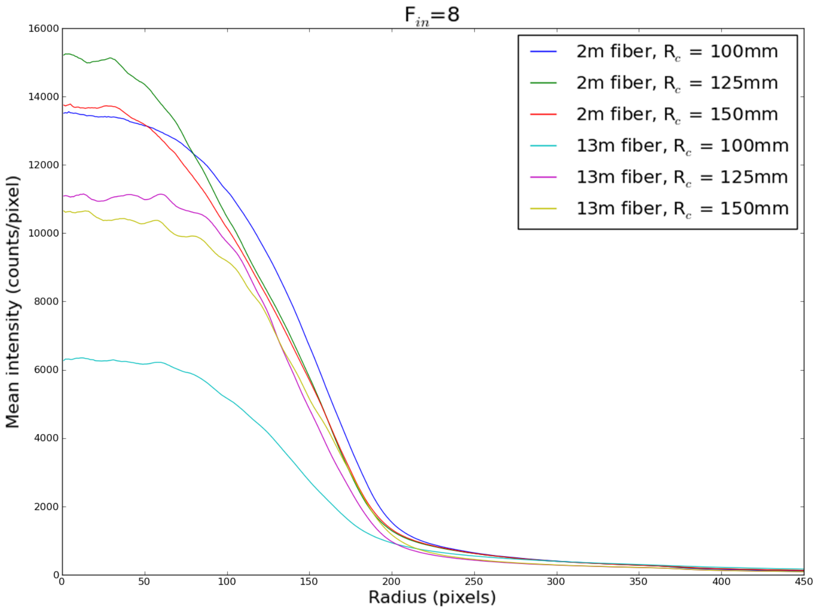

Figure 15: Radial intensity plots for the different fibres and radii of curvature illuminated with an F/8 input beam

4.2 FRD measurements

As mentioned before, many other groups studied the FRD of optical fibres, nevertheless no uniform definition of the phenomenon has been given. This is mainly because the ways to determine FRD are different for each group and the purposes of the fibres measured are different and therefore the characteristics to be known different. In this research we will first show the measurements that are usefull for the system design for the Integral Field Unit. Apart from these results we will also show a plot which is comparable to plots from other groups.

For the design of the proposed Integral Field Unit we are interested in the collimator speed necessary to maximise the efficiency of the system and the dependence of this on the macrobends that are unavoidable in the mechanical design of the instrument. Since the collimator speed, and thus its size, affects the resolution of the spectrograph, this trade off needs to be studied carefully. Figures 16 and 17 show the output focal ratio for two different fibres as a function of the input focal ratio for different percentages of light and different radii of curvature. Meaning that at the 50% line, just 50% of the transmitted light is caught in the output focal ratio cone. The same but with different percentages applies to the other lines.

Figure 19 summarises the results of figures 16 and 17, but are only for the measurements where an F/8 input beam was used. This is interesting for our research since our telescope also has an F/8 output beam. Note again that the R_c = 100 mm for the 13 metre fibre significantly differs from the other measurements. This is, as mentioned before, caused by microbends or by the way of rolling up the fibre.

In Figure 18 the input focal ratio is plotted against the output focal ratio. In this figure the output ratio is defined by the full width half maximum.

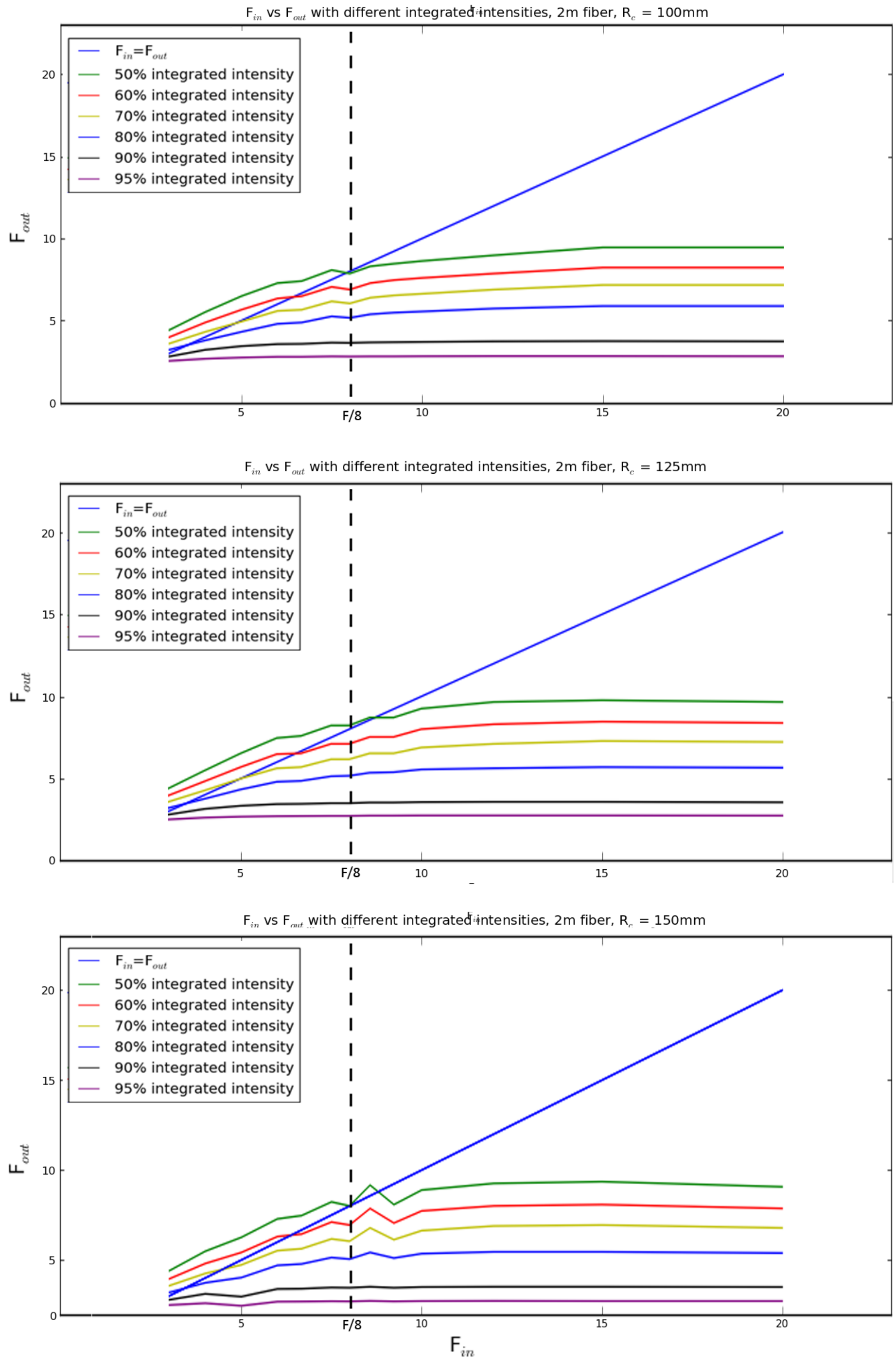

Figure 16: F$_{in}$ vs. F$_{out}$ for a 2 metre fibre with Radius of Curvature of 100, 125 and 150 mm

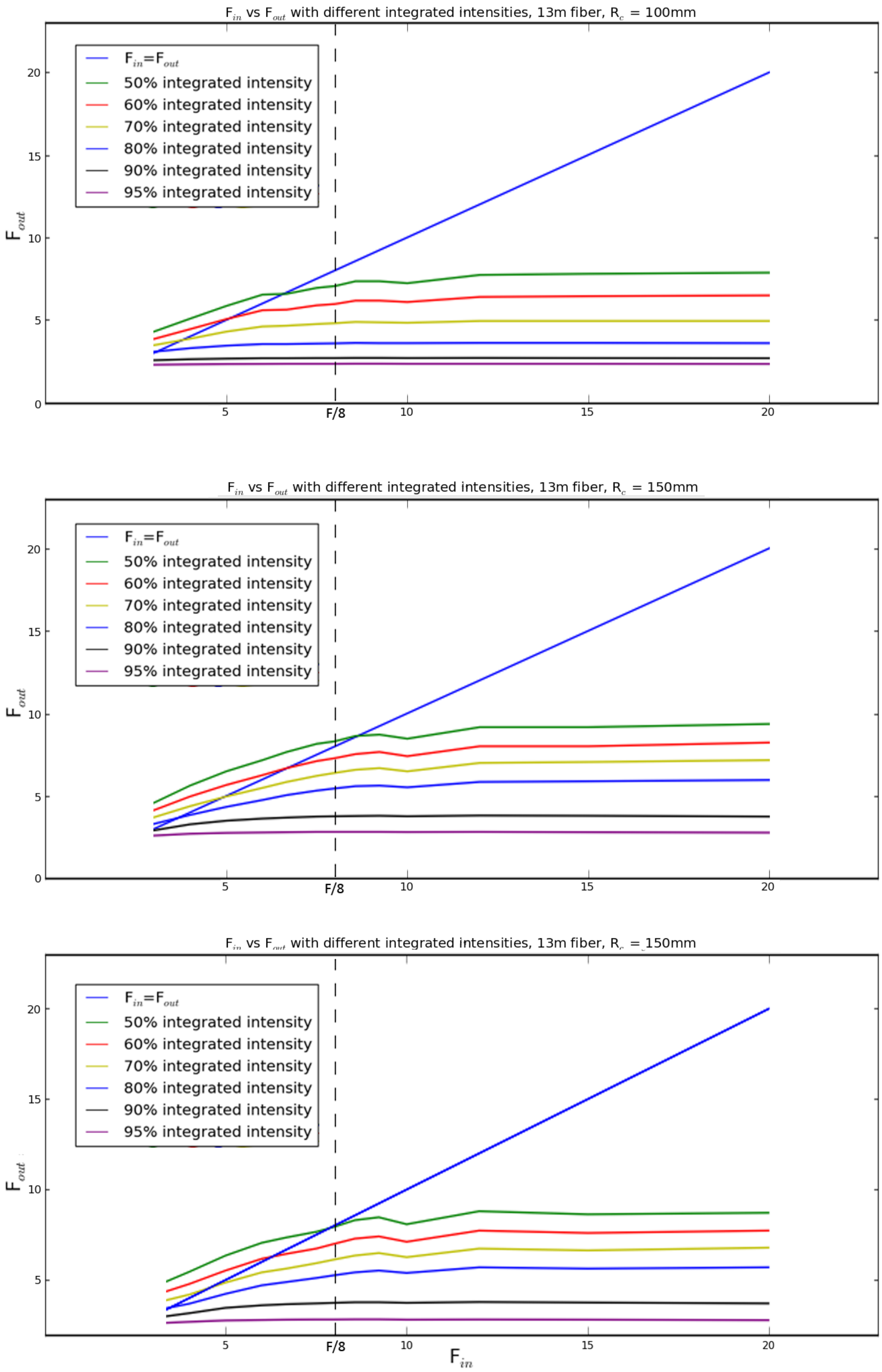

Figure 17: F_{in} vs. F_{out} for a 13 metre fibre with Radius of Curvature of 100, 125 and 150mm

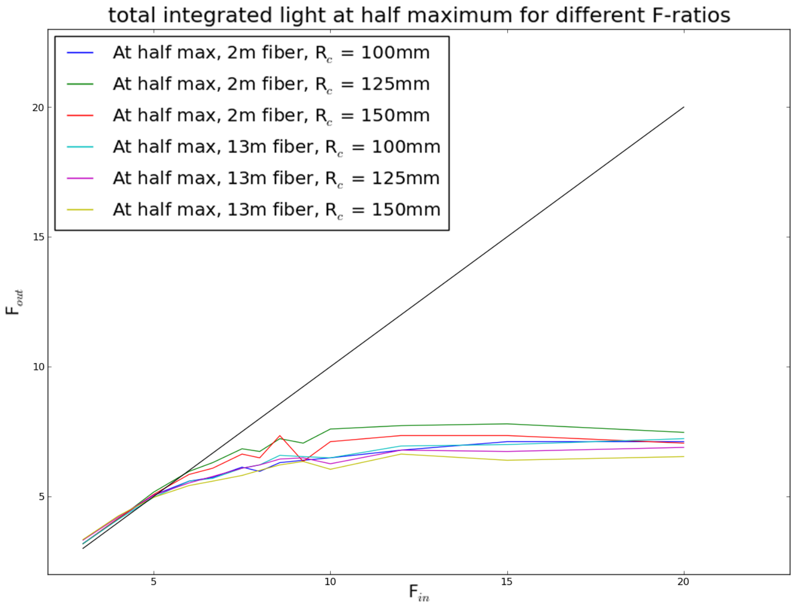

Figure 18: Input F/# against output F/# at full width half maximum for the measurements done

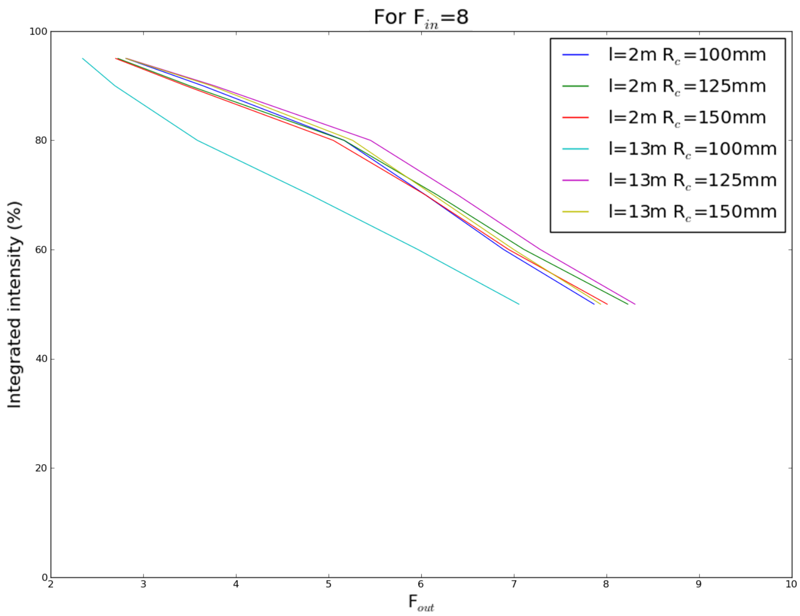

Figure 19: Relative percentages of light vs. the collimator speed, X-axis for different lengths and Radii of curvature, for an F/8 input beam

5 Discussion and conclusion

5.1 Light losses

As described in section 3.4, the exposure times were adjusted to the diafragma aperture sizes to make sure that the amount of light falling onto the fibre remains constant for each measurement. In table 4.1 it can be seen that, with these adjusted integration times, the total intensity is measured to be within a range of 10%. From this we can conclude that no significant amount of light is lost in the optical system and that background issues do not play a significant role in the performed measurements.

However the throughput for the 2 metre and 13 metre fibre differs. The 13 metre fibre propagates only 66% of the light propagated by the 2 metre fibre. From the product specifications in appendix A we can see that on average the losses in the window we are using are around 8 dB/km. The difference in fibre lengths is 11 metres. The loss expressed in dB would thus be 0.088 dB. While the fibre loss is measured te be 0.17 dB. This measured loss is roughly two times what we expect from the fibre characteristics. An explanation can be found in the fact that the 13 metre fibre was rolled up (with a big radius of curvature) during the measurements to store the long fibre. These twists made by the fibre might result in more lossy modes. Due to the fact that modes get reflected in lossy modes in a fibre when macrobended, see section 2.3. Due to space limits it was unfortunately not possible to position the fibre in such a way that rolling up the fibre could have been avoided.

5.2 FRD measurements

The purpose of this research was to determine the FRD for the given fibre and its dependence on fibre length and radius of curvature. From figures 16 and 17 we can see that there is barely any FRD dependence on the radius of curvature within the range of radii we tested. Only the 13 metre fibre with $R_c = 100$ mm is influenced, this is probably due to the fact that the fibre was rolled up many times with a radius of 100 mm, or because of microbends which were caused by fixing the fibre in this radius of curvature. The fibres are mechanically limited to bend no more than 125 mm by the anti-kink pipes that are to be used in the final instrument. Therefore can conclude that the bending of the fibres by the movement of the telescope will not significantly influence the FRD of the fibre and therefore the efficiency of the optical system as a whole.

As expected from the literature, the length of the fibre only has a small impact on the FRD properties of the fibre. For the optical design of the IFU this is not relevant since only the measurements of the 13 metre fibre will be used. Nevertheless it was good to verify that the results of our measurements with different fibre lengths agree with the literature.

5.3 Comparison with other results

The results presented in the previous section can be compared with other research done in the field. As mentioned, many different definitions are used for FRD but in a paper by Samuel C. Barden [12], similar measurements and a similar plot are presented. Figure 20 shows the plot by Barden.

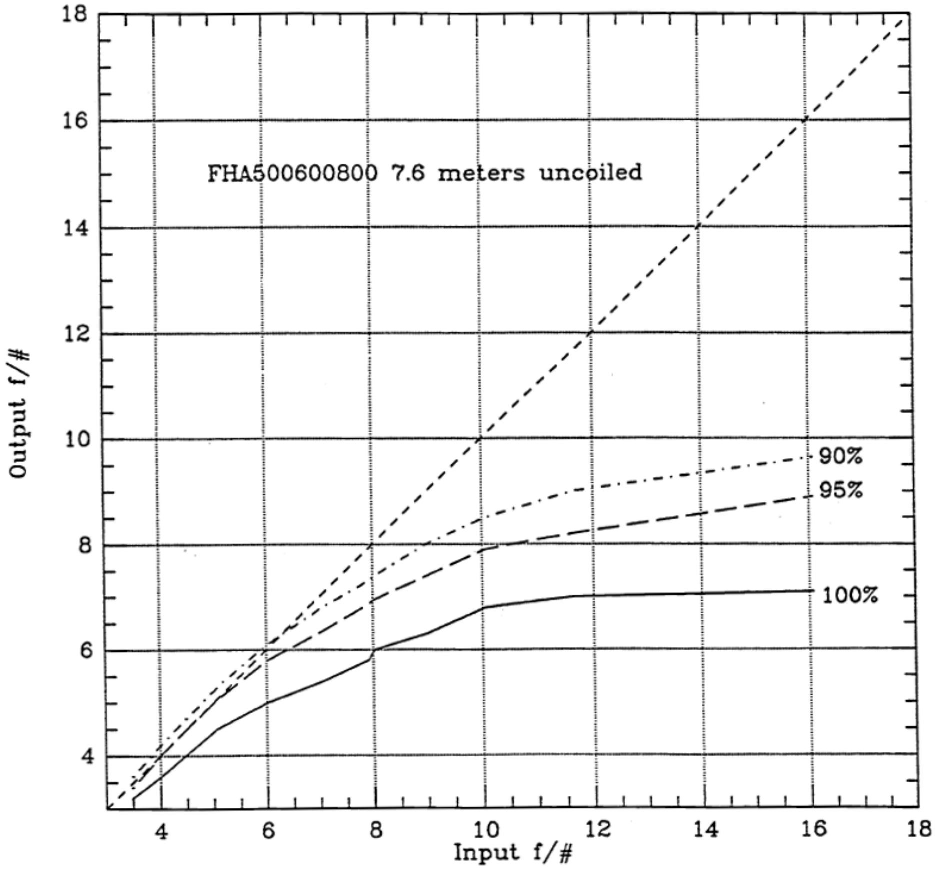

Figure 20: "Output focal ratio versus input focal ratio for a 7.6 meter fiber. The ideal case is indicated by the straight, dashed line. The curves indicate the speed of the collimator required to collect the indicated percentage of light as a function of input focal ratio." [12]

As can be seen in the figure by Barden, the measurements show a similar trend compared to what we find in the measurements done in our research. A radical difference is that the trend found by Barden only applies to lower percentages of light in our research. This effect seems to be inherent to our way of measuring the FRD. A possible explanation is that we consistently overestimate the light at higher radii, which is not unrealistic since we extrapolate the light for these high radii as explained in the section about the data reduction. To get around this uncertainty, additional optics have to be applied inbetween the fibre end and the CCD, or a larger CCD is needed.

The fact that the focal ratio slows down for fast input beams is unexpected and does not agree with the literature. Also in the paper by Barden this is the case for the 90% line. This unexpected result in both the paper by Barden and our research seems to be inherent to the definition of the focal ratio. Still, our result is rather usefull since these plots give a good indication of what the focal ratio of the collimator needs to be in order to maximise the efficiency of the system.

A better definition for FRD seems to be the full width at half maximum, as can be seen in figure 18. This definition does not give unexpected output FRD's. The drawback is that no information is given about the amount of light collected by a collimator speed. The plots in figure 16 and 17 do give information on the amount of light collected by a collimator with a speed as indicated on the x-axis and are therefore more applicable to meet the goal of our research.

5.4 Recommendations for further research

Since we were limited in resources for the experimental set-up, we had to limit ourselves to relative measurements. To get a better understanding of the implications of the fibre in the optical system of the IFU, absolute measurements would be more reliable to determine the collimator speed and the amount of light it will collimate.

The CCD used was limited in size. Especially the measurements for fast input beams were not always reliable. For further research, fore optics to reduce the size of the output beam of the fibre might be useful. However, extra optics means more light losses.

As mentioned earlier in the report, the measurements on the 13 metre fibre with a radius of curvature of 100mm show different outcomes than expected. It would be nice to reproduce these measurements to verify the outcomes to limit the effects of microbends. Another technique of rolling up the fibre might also influence the outcome and should therefore be further investigated.

In the described experimental set-up, the fibres are connected differently than will be the case for the IFU. Since microbends also contribute to FRD, it would be interesting to test the fibres again when they are bundled and installed for operation. The results will then be more applicable to the final instrument.

References

[1] Book: *Introduction to Fiber Optics (3rd Edition)* John Crisp, Barry Elliott (2005), ISBN 0 7506 67567

[2] Verheijen, M., Bershady, M., Andersen, D., Swaters, R., Westfall, K., Kelz, A. and Roth, M. (2004) *The Disk Mass project; science case for a new PMAS IFU module.* Astronomische Nachrichten, 325: 151–154. doi: 10.1002/asna.200310197,

[3] J.R.P. Angel, M.T. Adams, T.A. Boroson and R.L. Moore, (1977) *A very large optical telescope array linked with fused silica fibers* Apj 218:776-782

[4] C.A. Clayton (1989) *The implications of image scrambling and focal ratio degradation in fibre optics on the design of astronomical instrumentation* Astronomy and Astrophysics (ISSN 0004-6361), vol. 213, no. 1-2, April 1989, p. 502-515. Research supported by SERC., 1989A&A...213..502C

[5] Esperanza Carrasco and Ian R. Parry (1994) *A method for determining the focal ratio degradation of optical fibres for astronomy* Mon. Not. R. Astron. Soc., 271, 11994MNRAS.271....1C

[6] Ramsey, L. W. (1988) *Focal ratio degradation in optical fibers of astronomical interest* Fiber optics in astronomy; Proceedings of the Conference, Tucson, AZ, Apr. 11-14, 1988 (A90-20901 07-35). San Francisco, CA, Astronomical Society of the Pacific, 1988, p. 26-39; Discussion, p. 40. Research supported by Pennsylvania State University., 1988ASPC....3...26R

[7] Craig, W. W., Hailey, C. J., & Brodie, J. P. (1988) *Measurement of fibers to be used in fiber fed spectroscopy* Fiber optics in astronomy; Proceedings of the Conference, Tucson, AZ, Apr. 11-14, 1988 (A90-20901 07-35). San Francisco, CA, Astronomical Society of the Pacific, 1988, p. 41-51. Research supported by Lawrence Livermore National Laboratory., 1988ASPC....3...41C

[8] M.M. Roth, A. Kelz, T. Fechner, T. Hahn, S.-M. Bauer, T. Becker, P. Boehm, L. Christensen, F. Dionies, J. Paschke, E. Popow, D. Wolter, J. Schmoll, U. Laux, W. Altmann (2005) *PMAS, the Potsdam Multi-Aperture Spectrophotometer. I. Design, Manufacture, and Performance* PASP, arXiv:astro-ph/0502581v1

[9] Andreas Kelz, Marc A.W. Verheijen, Martin M. Roth, Svend M. Bauer, Thomas Becker, Jens Paschke, Emil Popow, Sebastian F. Sanchez, Uwe Laux (2005) *PMAS: The Potsdam Multi Aperture Spectrophotometer. II. The Wide Integral Field Unit PPak* PASP, arXiv:astro-ph/0512557v1

[10] Matthew A. Bershady, David R. Andersen, Justin Harker, Larry W. Ramsey, Marc A. W. Verheijen (2004) *SparsePak: A Formatted Fiber Field Unit for The WIYN Telescope Bench Spectrograph. I. Design, Construction, and Calibration* PASP, arXiv:astro-ph/0403456v1

[11] Matthew A. Bershady, David R. Andersen, Marc A. W. Verheijen, Kyle B. Westfall, Steven M. Crawford and Rob A. Swaters (2005) *SparsePak: A Formatted Fiber Field Unit for The WIYN Telescope Bench Spectrograph. II. On-Sky Performance* ApJS 156 311 doi: 10.1086/426479

[12] Samuel C. Barden (1995) *Review of fiber optic properties for astronomical spectroscopy* Proc. SPIE Vol. 2476, p. 2-9

A Fibre Specifications

SILICA/SILICA Optical Fiber FBP

- FBP: Broad Spectrum Optical Fiber
- Solarization Resistant

Fibers

Characteristics

- New Lower Loss Broad Spectrum Fiber, 275-2100nm
- Excellent Focal Ratio Degradation Characteristics
- Step Index
- Numerical Aperture: 0.22 ± 0.02
- Silica Core, Doped Silica Clad
- Cost Effective
- Polyimide Concentricity ± 3µm
- Tight Tolerance
- Operating Temperature: −65°C to +300°C
- Proof Tested to 100kpsi
- Custom Sizes, Buffers, Jackets, Assemblies Available

This fiber is designed to operate over a very broad range of wavelengths. It is produced with a Patent Pending process that allows more flexibility to meet smaller quantity requests for a variety of core:clad ratios.

Product Descriptor	Core (µm)	Clad (µm)	Buffer (µm)
FBP200220240	200 ± 4	220 ± 4	239 ± 5
FBP300330370	300 ± 6	330 ± 7	370 ± 10
FBP400440480	400 ± 8	440 ± 9	480 ± 7
FBP500550590	500 ± 10	550 ± 10	590 ± 10
FBP600660710	600 ± 10	660 ± 10	710 ± 10
FBP100120140	100 ± 3	120 ± 3	140 ± 4
FBP200240280	200 ± 4	240 ± 4	275 ± 5
FBP320385415	320 ± 8	385 ± 8	415 ± 10
FBP050070085	50 ± 2	70 ± 2	90 ± 3
FBP100140170	100 ± 3	140 ± 3	170 ± 5

Typical Attenuation

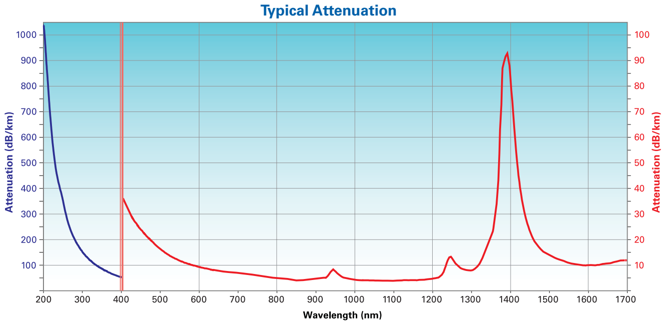

Polymicro Technologies, LLC
QUALITY MANAGEMENT SYSTEM CERTIFIED BY DNV ISO 9001:2000
18019 N. 25th Avenue • Phoenix, AZ 85023-1200
Voice: (602) 375-4100 Fax: (602) 375-4110
E-Mail: sales@polymicro.com
URL: http://www.polymicro.com

- Flexible Capillary
- Multimode Optical Fiber
- Specialty Assemblies
- Micro-Components

PT-FBP/12-04

Figure 21: Product specifications fibres

B Quantum Efficiency

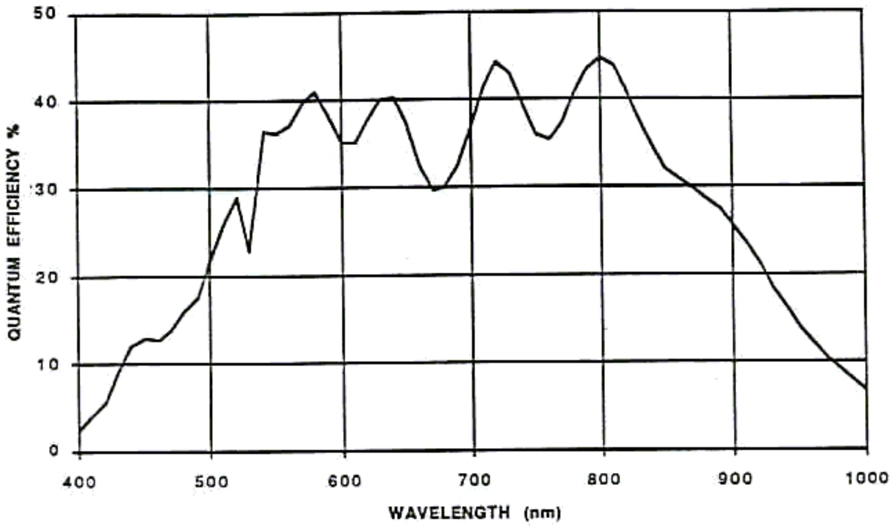

Figure 22: Quantum efficiency vs. wavelength for the kaf400 CCD used in this research